

Photoacoustic signal enhancements from gold nano-colloidal suspensions excited by a pair of time-delayed femtosecond pulses

Frances Camille P. Masim,¹ Wei-Hung Hsu,¹ Hao-Li Liu,² Tetsu Yonezawa,³ Armandas Balčytis,^{4,5} Saulius Juodkazis,^{4,6} and Koji Hatanaka^{1,*}

¹Research Center for Applied Sciences, Academia Sinica, 128 Sec. 2, Academia Rd., Nankang, Taipei 115, Taiwan (R. O. C.)

²Department of Electrical Engineering, Chang Gung University, 259, Wenhua 1st Rd., Guishan Dist., Taoyuan 333, Taiwan (R. O. C.)

³Division of Materials Science and Engineering, Faculty of Engineering, Hokkaido University, Kita 13 Nishi 8, Kita-ku, Sapporo, 0608628, Japan

⁴Nanotechnology Facility, Center for Micro-Photonics, Swinburne University of Technology, John St., Hawthorn, VIC 3122, Australia

⁵Center for Physical Sciences and Technology, Savanorių Ave. 231, LT-02300 Vilnius, Lithuania

⁶Melbourne Centre for Nanofabrication, the Victorian Node of the Australian National Fabrication Facility, 151 Wellington Rd., Clayton 3168 Vic, Australia

*kojihntk@gate.sinica.edu.tw

Abstract: Photoacoustic signal enhancements were observed with a pair of time-delayed femtosecond pulses upon excitation of gold nanosphere colloidal suspension. A systematic experimental investigation of photoacoustic intensity within the delay time, $\Delta t = 0$ to 15 ns, was carried out. The results revealed a significant enhancement factor of ~ 2 when the pre-pulse energy is 20-30% of the total energy. Pre-pulse and main pulse energy ratios, $E_p^{(1)}:E_s^{(2)}$, were varied to determine the optimal ratio that yields to maximum photoacoustic signal enhancement. This enhancement was ascribed to the initial stage of thermalization and bubble generation in the nanosecond time scale. Pre-pulse scattering intensity measurements and numerical finite-difference time-domain calculations were performed to reveal dynamics and light field enhancement, respectively.

© 2021 Optical Society of America

OCIS codes: (110.5125) Photoacoustics; (140.7090) Ultrafast lasers; (160.4236) Nanomaterials; (240.6680) Surface Plasmons; (320.2250) Femtosecond Phenomena

References and links

1. G. Du, Q. Yang, F. Chen, Y. Ou, Y. Wu, and X. Hou, "Ultrafast dynamics of laser thermal excitation in gold film triggered by temporally shaped double pulses," *Int. J. Ther. Sci.* **90**, 197 – 202 (2015).
2. T. Kumada, T. Otohe, M. Nishikino, N. Hasegawa, and T. Hayashi, "Dynamics of spallation during femtosecond laser ablation studied by time-resolved reflectivity with double pump pulses," *Appl. Phys. Lett.* **108**, 011102 (2016).
3. Y. Ou, Q. Yang, G. Du, F. Chen, Y. Wu, Y. Lu, and X. Hou, "Ultrafast thermalisation dynamics in Au film excited by a polarization-shaped femtosecond laser double-pulse," *Opt. Laser Tech.* **70**, 71 – 75 (2015).

4. S. Danworaphong, T. A. Kelf, O. Matsuda, M. Tomada, Y. Tanaka, O. B. Wright, Y. Nishijima, L. Ueno, S. Juodkazis, and H. Misawa, "Real-time imaging of acoustic rectification" *Appl. Phys. Lett.* **99**, 201919 (2011).
5. J. Mildner, C. Sarpe, N. Gotte, M. Wollenhaupt, and T. Baumert, "Emission signal enhancement of laser ablation of metals (aluminum and titanium) by time delayed femtosecond double pulses from femtoseconds to nanoseconds," *Appl. Sur. Sci.* **302**, 291 – 298 (2014).
6. J. Penczak, R. Kupfer, I. Bar, and R.J. Gordon, "The role of plasma shielding in collinear double-pulse femtosecond laser-induced breakdown spectroscopy," *Spectro. Act. Part B* **97**, 34 – 41 (2014).
7. T. Somekawa, M. Otsuka, Y. Maeda, and M. Fujita, "Signal enhancement in femtosecond laser induced breakdown spectroscopy with a double-pulse configuration composed of two polarizers," *Jap. J. Appl. Phy.* **55**, 058002 (2016).
8. V. I. Babushok, F. C. De Lucia Jr., J. A. Gottfried, C. A. Munson, and A. W. Miziolek, "Double pulse laser ablation and plasma: Laser induced breakdown spectroscopy signal enhancement," *Spectro Acta B.* **61**, 999 – 1014 (2006).
9. J. R. McLaughlan, R. A. Roy, H. Ju, and T. W. Murray, "Ultrasonic enhancement of photoacoustic emissions by nanoparticle-targeted cavitation," *Opt. Letters* **35**(13), 2127 – 2129 (2010).
10. J. D. Dove, T. W. Murray, and M. A. Borden, "Enhanced photoacoustic response with plasmonic nanoparticle-templated microbubbles," *Soft Matter* **9**, 7743 – 7750 (2013).
11. M. Jeon, W. Song, E. Huynh, J. Kim, B. L. Helfield, B. Y. C. Leung, D. E. Geortz, G. Zheng, J. Oh, J. F. Lovell, C. Kim, "Methylene blue microbubbles as a model dual-modality contrast agent for ultrasound and activatable photoacoustic imaging," *J. Biomed. Optics* **19**(1), 06005 (2014).
12. H. Moon, D. Kumar, H. Kim, C. Sim, J.-H. Chang, J. -M. Kim, H. Kim, and D. -K. Lim, "Amplified photoacoustic performance and enhanced photothermal stability of reduced graphene oxide coated gold nanorods to sensitive photoacoustic imaging," *ACS Nano* **9**(3), 2711 – 2719 (2015).
13. C. -W. Wei, M. Lomardo, K. Larson-Smith, I. Pelivanov, C. Perez, J. Xia, T. Matula, D. Pozzo, and M. O'Donnell, "Nonlinear contrast enhancement in photoacoustic molecular imaging with gold nanosphere encapsulated nanoemulsions," *Appl. Phys. Lett.* **104**, 033701 (2014).
14. E. Huynh, J. F. Lovell, B. L. Helfield, M. Jeon, D. E. Geortz, B. C. Wilson, and G. Zheng, "Porphyrin shell microbubbles with intrinsic ultrasound and photoacoustic properties," *J. Am. Chem. Soc.* **134**(40), 16464 – 16467 (2012).
15. K. Wilson, K. Homan, and S. Emelianov, "Biomedical photoacoustics beyond thermal expansion using triggered nanodroplet vaporization for contrast-enhanced imaging," *Nat. Comm.* **3**, 1 – 10 (2012).
16. K. Metwally, S. Mensah, and G. Baffou, "Fluence threshold of photothermal bubble generation using plasmonic nanoparticles," *J. Phys. Chem. C.* **119**, 28586 – 28596 (2015).
17. C. Boutopoulos, A. Hatef, M. Fortin-Deschenes, and M. Meunier, "Dynamic imaging of a single gold nanoparticle in liquid irradiated by off-resonance femtosecond laser" *Nanoscale* **7**, 11758 – 11765 (2015).
18. A. Plech and V. Kotaidis, "Laser-induced heating and melting of gold nanoparticles studied by time-resolved x-ray scattering" *Phys. Rev. B.* **70**, 195423 (2004).
19. A. Siems, S.A.L. Weber, J. Boneberg, and A. Plech, "Thermodynamics of nanosecond nanobubble formation at laser-excited metal nanoparticles" *New Journal of Physics* **13**, 043018 (2011).
20. R. Lachaine, C. Boutopoulos, P. Lajoie, E. Boulais, and M. Meunier, "Rational design of plasmonic nanoparticles for enhanced cavitation and cell perforation," *Nano Lett.* **16**, 3187 – 3194 (2016).
21. R. Lachaine, E. Boulais, D. Rioux, C. Boutopoulos, and M. Meunier, "Computational design of durable spherical nanoparticles with optimal material, shape, and size for ultrafast plasmon-enhanced nanocavitation," *ACS Photonics* **3**, 2158 – 2169 (2016).
22. H. F. Zhang, K. Maslov, G. Stoica, and L. V. Wang "Functional photoacoustic microscopy for high-resolution and noninvasive in vivo imaging," *Nat. Biotechnol.* **24**, 848 – 851 (2006).
23. T. T. W. Wong, R. Zhang, P. Hai, C. Zhang, M. A. Pleitez, R. B. Aft, D. V. Novack, and L. V. Wang, "Fast label-free multilayered histology-like human breast cancer by photoacoustic microscopy," *Sci. Advances* **3**, e1602168 (2017).
24. B. E. Urban, J. Yi, V. Yakovlev, and H. F. Zhang, "Investigating femtosecond-laser-induced two-photon photoacoustic generation," *J. Biomed. Optics* **19**(8), 085001 (2014).
25. R. Zhang, B. Rao, H. Rong, B. Raman, and L. V. Wang "In vivo photoacoustic neuronal imaging of odor-evoked calcium signals in disophila brain," *Proc. of SPIE* **9708**, (2016).
26. X. Wang, Y. Pang, G. Ku, X. Xie, G. Stoica, and L.V. Wang, "Noninvasive laser-induced photoacoustic tomography for structural and functional in vivo imaging of the brain," *Nat. Biotechnol.* **21**, 803 – 806 (2003).
27. M. Muramatsu, T.-F. Shen, W.-Y. Chiang, A. Usman, and H. Masuhara, "Picosecond motional relaxation of nanoparticles in femtosecond laser trapping," *J. Phys. Chem. C* **120**, 5251 – 5256 (2016).
28. Y. Lu, Q. Yang, F. Chen, G. Du, Y. Wu, Y. Ou, and X. Hou, "Ultrafast near-field enhancement dynamics in a resonance-mismatched nanorod excited by temporally-shaped femtosecond laser double pulses," *Opt. Laser Tech.* **77**, 6 – 10 (2016).
29. H. Zhang, Z. Hu, Z. Ma, M. Gecevicius, G. Dong, S. Zhou, and J. Qiu, "Anisotropically enhanced nonlinear optical properties of ensembles of gold nanorods electrospun in polymer nanofiber film," *ACS Appl. Mater.*

- Interfaces **8**, 2048 – 2053 (2016).
30. T. Zhao, J.W. Jarrett, J.S. Johnson, K. Park, R.A. Vaia, and K.L. Knappenberger, Jr., “Plasmon dephasing in gold nanorod studied using single-nanoparticle interferometric nonlinear optical microscopy,” *J. Phys. Chem. C* **120**, 4071 – 4079 (2016).
 31. M. Hu, H. Petrova, and G.V. Hartland, “Investigation of the properties of gold nanoparticles in aqueous solution at extremely high lattice temperatures,” *Chem. Phys. Lett.* **391**, 220 – 225 (2004).
 32. F.C.P. Masim, M. Porta, W.-H. Hsu, M. T. Nguyen, T. Yonezawa, A. Balcytis, S. Juodkazis, and K. Hatanaka, “Au Nanoplasma as efficient hard X-ray emission source,” *ACS Photonics* **3**, 2184 – 2190 (2016).
 33. F.C.P. Masim, H. L. Liu, M. Porta, T. Yonezawa, A. Balcytis, S. Juodkazis, W. -H. Hsu, and K. Hatanaka, “Enhanced photoacoustics from gold nano-colloidal suspensions under femtosecond laser excitation,” *Opt. Express* **24**(13), 14781 – 14792 (2016).
 34. F.C.P. Masim, W.-H. Hsu, C. H. Tsai, H. -L. Liu, M. Porta, M. T. Nguyen, T. Yonezawa, A. Balcytis, X. Wang, S. Juodkazis, and K. Hatanaka, “MHz-ultrasound generation by chirped femtosecond laser pulses from gold nano-colloidal suspensions,” *Opt. Express* **24**(15), 17050 – 17059 (2016).
 35. Q. Wang, S. Luo, Z. Chen, H. Qi, J. Deng, and Z. Hu, “Drilling of aluminum and copper films with femtosecond double-pulse laser,” *Opt. Laser Tech.* **80**, 116 – 124 (2016).
 36. A. Chen, Y. Wang, L. Sui, S. Li, S. Li, D. Liu, Y. Jiang, and M. Jin, “Optical emission generated from silicon under dual-wavelength femtosecond double-pulse laser irradiation,” *Opt. Express* **23**(19), 24650 – 24656 (2015).
 37. G. Vogt, P. Nuernberger, R. Selle, F. Dimler, T. Brixner, and G. Gerber, “Analysis of femtosecond quantum control mechanisms with colored double pulses,” *Phys. Rev. A* **74**, 033413 (2006).
 38. V. Pinon, C. Fotakis, G. Nicolas, and D. Anglos, “Double pulse laser-induced breakdown spectroscopy with femtosecond laser pulses,” *Spectro. Acta. Part B* **63**, 1006 – 1010 (2008).
 39. V. Pinon, C. Fotakis, G. Nicolas, and D. Anglos, “Optimization of collinear double-pulse femtosecond laser-induced breakdown spectroscopy of silicon,” *Spectro. Acta. Part B* **62**, 1412 – 1418 (2007).
 40. J. Guo, T. Wang, J. Shao, T. Sun, R. Wang, A. Chen, Z. Hu, M. Jin, and D. Ding, “Emission enhancement ratio of metal irradiation by femtosecond double-pulse laser,” *Optics Comm.* **285**, 1895–1899 (2012).
 41. S. S. Harilal, P. K. Diwakar, and A. Hassanein, “Electron-ion relaxation time dependent signal enhancement in ultrafast double-pulse laser-induced breakdown spectroscopy,” *Appl. Phys. Lett.* **103**, 041102 (2013).
 42. P.A. Benedetti, G. Cristoforetti, S. Legnaioli, V. Palleschi, L. Pardini, A. Salvetti, and E. Tognoni, “Effect of laser pulse energies in laser induced breakdown spectroscopy in double-pulse configuration,” *Spectro. Acta. Part B* **60**, 1392 – 1401 (2005).
 43. A. De Giacomo, M. Dell’Aglia, O. De Pascale, and M. Capitelli, “From single pulse to double pulse ns-laser induced breakdown spectroscopy under water: Elemental analysis of aqueous solutions and submerged solid samples,” *Spectro. Acta. Part B* **62**, 721 – 738 (2007).
 44. J. Scaffidi, J. Pender, W. Pearman, S.R. Goode, B.W. Colstron, Jr., J. Chance Carter, and S. Michael Angel “Dual-pulse laser-induced breakdown spectroscopy with combinations of femtosecond and nanosecond laser pulses,” *Appl. Optics* **42**(30), 6099 – 6106 (2003).
 45. N. G. Bastus, J. Comenge, and V. Puentes, “Kinetically controlled seeded growth synthesis of citrate-stabilized gold nanoparticles of up to 200 nm: size focusing versus Ostwald ripening,” *Langmuir* **27**, 11098 – 11105 (2011).
 46. N. R. Jana, L. Gearheart, and C. J. Murphy, “Seed-mediated growth approach for shape-controlled synthesis of the spherical and rod-like gold nanoparticles using a surfactant template,” *Adv. Materials* **13**(18), 1389 – 1393 (2001).
 47. T. Nakajima, X. Wang, S. Chatterjee, and T. Sakka, “Observation of number-density dependent growth of plasmonic nanobubbles” *Sci. Reports* **6**, 28667 (2016).
 48. E. Boulais, R. Lachaine, and M. Meunier, “Plasma-mediated nanocavitation and photothermal effects in ultrafast laser irradiation of gold nanorods in water” *J. Phys. Chem. C.* **7**, 9386 – 9396 (2013).
 49. R. Lachaine, E. Boulais, and M. Meunier, “From thermo- to plasma-mediated ultrafast laser-induced plasmonic nanobubbles” *ACS Photonics* **1**, 331 – 336 (2014).
 50. M. Malinauskas, A. Žukauskas, G. Bičkauskaitė, R. Gadonas, and S. Juodkazis, “Mechanisms of three-dimensional structuring of photo-polymers by tightly focused femtosecond laser pulses,” *Opt. Express* **18**(10), 10209–10221 (2010).
 51. K. Hatanaka, T. Ida, H. Ono, S.-I. Matsushima, H. Fukumura, S. Juodkazis, and H. Misawa, “Chirp effect in hard X-ray generation from liquid target when irradiated by femtosecond pulses,” *Opt. Express* **16**(17), 12650–12657, (2008).
-

1. Introduction

Recent studies on femtosecond (fs) laser-induced dielectric breakdown have gained a widespread interest in the fabrication of micro- and nano-functional devices [1–3] and real-time high resolution imaging due to its high emission frequency [4]. Fs-laser ablation offers significant advantages over nanosecond laser ablation such as a high precision with less of

thermal damage and a high reproducibility [5, 6]. On this basis, fs-laser pulses are suitable to improve high spatial resolution and sensitivity in biomedical photoacoustic imaging and photothermal therapy [7, 8]. Photoacoustic technique is one of the most promising biophotonic diagnostic modalities that incorporates non-ionizing radiation, non-invasive imaging, high spatial resolution, and deep penetration depth [9–11]. Photoacoustic signals are usually generated by one of the four mechanisms: thermal expansion, vaporization, chemical reaction induced by light, or optically induced dielectric breakdown [12]. Thermal expansion that is accompanied by cavitation generation results in efficient photoacoustic signal generation [13–15]. Formation mechanisms and dynamics of nano-bubbles around nanoparticles under pulsed laser irradiation are better understood following high resolution optical and X-ray imaging [16–19] and opened applications in cell laser optoporation and photothermal therapy [20, 21].

The existing high-resolution optical imaging modalities such as confocal microscopy, two-photon microscopy, and optical coherence tomography limit its applications on deep penetration imaging due to optical scattering. Compared with these imaging techniques, photoacoustic imaging is known to surpass the optical diffusion limit, providing a deeper penetration imaging with high spatial resolution [22–24]. It is considered to be a potential imaging tool in neuroscience which allows penetration in thick brain tissue. In vivo studies on noninvasive transdermal and transcranial imaging of the structure and function of rat brains by laser-induced photoacoustic tomography were reported [25, 26]. It allows accurate mapping of brain structures and functional cerebral hemodynamic changes in blood vessels. This neuroimaging modality is promising for significant applications in neurophysiology, neuropathology and neurotherapy.

Plasmonic gold nanoparticles are attractive in photoacoustics since they offer strong optical absorption when excited at the surface plasmon resonance wavelength. Nanoparticle-facilitated absorption of pulsed laser leads to a rapid and localized heating, which results in photoacoustic signal generation produced through thermo-elastic effect and cavitation generation [27–31]. The efficiency of optical absorption and photothermal conversion can be tuned through nanoparticle chemistry and geometry [32]. It has been demonstrated that enhanced photoacoustic intensity was observed by tuning the nanoparticle shape [33] and controlling the laser parameters such as pulse energy and temporal chirp [34].

However, with the use of single fs-laser pulse, the pulse parameters that influence the ablation process are circumscribed to the pulse energy and pulse width. To achieve effective control, double pulse, which contains two-polarized fs-pulses separated from femtoseconds to nanoseconds, has been widely used in control of light-matter interaction [35–37]. It was found that ablation can be precisely controlled by optimizing the number of pulses, pulse separation, and pulse energy ratio [38, 39]. Reports on semiconductor materials revealed that the ablation rate is higher for double-pulse compared to single-pulse irradiation of the same total fluence [40, 41]. Double pulse excitation leads to a better coupling of the laser beam with plasma and target material, thus providing a more temporally effective energy delivery to plasma and target material. This results in significant signal enhancements in the intensity emission lines up to two orders of magnitude larger than a conventional single pulse excitation [42–44].

Here, photoacoustic signal enhancements under double-pulsed (horizontally- and vertically-polarized) excitation to Au nanosphere colloidal suspensions were systematically investigated. Pre-pulse power dependence and different pre-pulse to main pulse energy ratios with the same total fluence were studied. The experimental results demonstrated that maximum enhancement is obtained at the optimal separation time between pulses and pulse energy ratios.

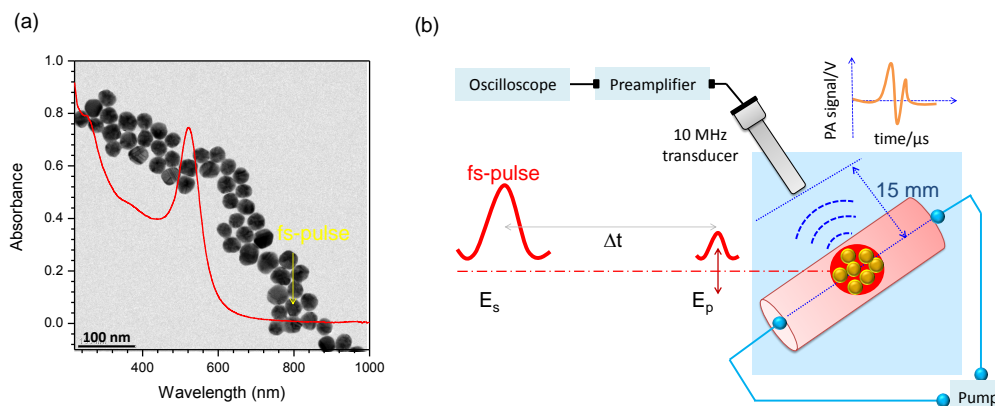


Fig. 1. (a) Absorption spectrum of Au nanosphere colloidal suspension with a strong characteristic absorption band at ~ 520 nm. TEM image of mono-dispersed colloidal suspension of Au nanosphere with a diameter of 20 nm is shown in the background. (b) Schematic diagram of the experimental setup for fs-double-polarized pulsed excitation to Au nanoparticle suspension for photoacoustic detection. Fs-laser pulses: pulse duration $t_0 = 40$ fs, central wavelength $\lambda = 800$ nm and pulse energy $E = 0.1$ mJ at 1 kHz repetition rate were focused inside the glass tube using $10\times$ numerical aperture $NA = 0.28$ objective lens. The pre-pulse was p-polarized while the main pulse was s-polarized. Distance between the focal spot and transducer was set at 15 mm in all experiments.

2. Samples and procedures

2.1. Synthesis of Au nanospheres

Colloidal suspensions of gold nanospheres for photoacoustic generation were prepared via synthesis described elsewhere [45, 46]. Briefly, a kinetically-controlled seeded growth synthesis of citrate-stabilized gold nanospheres was used. In a 250 mL three-necked round-bottomed flask, a solution of 2.2 mM sodium citrate in Milli-Q water (150 mL) was heated at 115°C for 15 min under vigorous stirring. A reflux condenser and an oil bath were used to prevent the evaporation of the solvent. After it reached the boiling point, 1 mL of $\text{HAuCl}_{4(aq)}$ (25 mM) was added. The color of the solution changed from yellow to bluish gray and then to light pink in 10 min. The resulting Au seed particles ~ 10 nm in diameter were coated with negatively charged citrate ions and completely dispersed in water. Immediately after the synthesis of the Au seed solution, the temperature was cooled down to 90°C and seeded growth of Au nanospheres was carried out. Then, 1 mL of $\text{HAuCl}_{4(aq)}$ solution (25 mM) was injected on the reaction vessel. The reaction was finished after 30 min and the process was repeated twice. After that, the sample was diluted by extracting 55 mL of the sample and adding 53 mL of Milli-Q water and 2 mL of 60 mM sodium citrate. This solution was then used as seed solution, and the process was repeated again. By changing the volume in each growth step, it is possible to tune the seed particle concentration. Mono-dispersed gold nanosphere colloidal suspensions with an absorption peak at ~ 520 nm corresponding to the diameter of 20 nm as shown in Fig. 1(a). Atomic concentration of $\sim 1.4 \times 10^{-4}$ mol/L, particle concentration of $\sim 3.5 \times 10^{14}$ NPs/L and volume of $\sim 4 \times 10^3$ nm³ were used in the experiments. Separation between particles estimated as a cubic

root of the volume-per-nanoparticle was $\sim 1.4 \mu\text{m}$. At this high-density, the formation and evolution of a nano-bubbles is directly affected by pressure waves encountered from surrounded nano-bubbles [47].

2.2. Femtosecond double-pulse configuration

Figure 1(b) shows a schematic diagram of the experimental setup of fs double-pulse experiments conducted using Ti:sapphire amplified laser system with pulse duration of $t_0 = 40 \pm 5$ fs, central wavelength of $\lambda = 800$ nm, and pulse energy of $E_p = 0.1$ mJ at 1 kHz repetition rate. Fs-laser pulses were directed through two cube polarizing beam splitters in order to create a pulse pair with s- and p-polarized beams. The first cube polarizing beamsplitter split the incoming laser pulse into two orthogonal optical paths while the second one was used to combine the beams after introducing time delay Δt between them in one of the arms. The delay was controlled automatically by mechanical stage with high precision. The maximum delay time range between the s- and p-polarized beams was 15 ns. A half waveplate which allows the rotation of the polarization vector was used to control the intensity ratio between the two polarized beams. The minimum s-pol. to p-pol. beam intensity ratio is 50/50, therefore measurements on pulse energy ratios with the same total fluence were restricted to 50/50, 60/40, 70/30, 80/20, 90/10, and 100/0. After the second cube polarizing beam splitter, the two polarized beams become collinear and were focused using $10\times$ numerical aperture $NA = 0.28$ objective lens. Two independent switches for s- and p-pol. beams were installed to control excitation under single pulse and double-pulse irradiation. For instance, in s-pol. beam irradiation, the p-pol. beam was blocked and vice versa. In contrary, under double-pulse excitation, both beams are present.

2.3. Photoacoustic detection and measurements

Femtosecond double-pulse with a total laser fluence of $1.05 \times 10^3 \text{ J/cm}^2$ were tightly-focused onto a 5-mm-diameter glass capillary tube inside the water tank which is used to circulate colloidal suspensions of gold nanoparticles. An off-resonance (laser wavelength $\lambda = 800$ nm does not coincide with the characteristic absorption band of Au nanosphere at $\lambda = 520$ nm) pulsed laser excitation of gold nanosphere colloidal suspensions was performed, proving a higher thermal stability of gold nanoparticles. For the photoacoustic detection and measurements, a single element unfocused ultrasound transducer (A312-N-SU) with a detection frequency of 10 MHz was used. The distance between the ultrasound transducer and glass tube was kept constant at 15 mm in the entire experiment. Photoacoustic signals were detected and amplified using an ultrasound preamplifier (5678, Olympus) and the acquired signals were recorded and analyzed using digital oscilloscope (DSO-X 3034A, Agilent Tech.). The geometry of glass capillary tube in water [Fig. 1(b)] was used to simulate the experiments with biomedical relevance where the photoacoustic signal generation is separated from detection. The first peak of the time-dependent photoacoustic signal which corresponds to the fundamental ultrasound signal was used as a measure of photoacoustic response from the fs laser-irradiated gold nanosphere colloidal suspensions. Then, the average of the measured photoacoustic signal intensities was determined for three experimental trials.

2.4. Pre-pulse scattering intensity measurements

Near-IR fs-laser pulses (horizontally-polarized) was focused onto a water-filled quartz cuvette, creating a super-continuum white light (SWL) with a broad band emission wavelength of $\lambda = 300 - 1000$ nm. The SWL was used as a strobe light to perform dark field imaging and scattering measurements on pre-pulse (vertically-polarized) excited gold nanosphere colloidal suspensions. The pre-pulse energy was maintained at $100 \mu\text{J}$ and its scattering intensity measurements were investigated throughout the time delay range of 0 to 15 ns. A photodiode

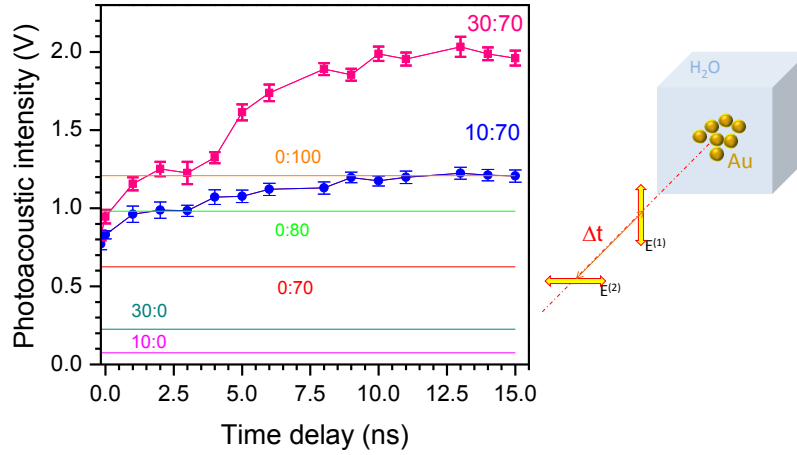


Fig. 2. Photoacoustic intensity as a function of time delay between fs-laser pulses vertically (p-pol.) and horizontally (s-pol.) from $\Delta t = 0$ to 15 ns delay. Pulse energy ratio of pre-pulse to the main pulse $E_p^{(1)} : E_s^{(2)}$ in μJ is shown at their approximate maximum signal levels.

was used as a detector for light scattering intensity measurements. The maximum scattering light intensity was observed at the wavelength $\lambda = 600$ nm, which was used as a basis for scattering intensity measurements.

3. Results

3.1. Photoacoustic intensity enhancement under double-pulse excitation

The photoacoustic intensity as a function of time delay between fs-laser pulses vertically (p-pol) and horizontally (s-pol) from $\Delta t = 0$ to 15 ns is shown in Fig. 2. The measurements of photoacoustic intensity were taken under single pulse (s-pol or p-pol) and double-pulse (s-pol and p-pol) excitation to Au nanosphere colloidal suspension. A significant increase in photoacoustic intensity was observed under polarized double-pulsed excitation ($E_p^{(1)} : E_s^{(2)} = 30:70 \mu\text{J}$ and $E_p^{(1)} : E_s^{(2)} = 10:70 \mu\text{J}$) as the time delay between pre-pulse $E_p^{(1)}$ and the main pulse $E_s^{(2)}$ increased from 0 to 15 ns. At $E_p^{(1)} : E_s^{(2)} = 30:70 \mu\text{J}$ (double-pulse), the photoacoustic intensity reached up to 3.2, 2.4 and 1.8 times higher than that of $E_s^{(2)} = 70 \mu\text{J}$ (main pulse), $E_p^{(1)} + E_s^{(2)} = 30 + 70 \mu\text{J}$ (sum of pre-pulse and main pulse), and $E_s^{(2)} = 100 \mu\text{J}$ (main pulse), respectively. When the pre-pulse intensity was decreased from 30 to 10 μJ , the photoacoustic intensity decayed 1.8 times. The significant enhancement in photoacoustic intensity under double-pulse excitation is attributed to the efficient photon energy coupling to nanoparticles at the nanosecond time scale due to the initial state of thermal expansion and generation of nano-bubbles (Sec. 4).

In Fig. 3, pulse energy ratios for the same total fluence as a function of photoacoustic intensity at different time delays ($\Delta t = 0, 2, 5, 10, 15$ ns) were systematically investigated. Different pulse energy ratios of $E_s^{(2)} : E_p^{(1)} = 100:0, 90:10, 80:20, 70:30, 60:40$ and $50:50 \mu\text{J}$ (same total fluence of $100 \mu\text{J}$) were used to determine the optimal ratio that could yield to the highest photoacoustic enhancement. At $\Delta t = 0$, the photoacoustic intensity was linearly dependent on the main pulse energy $E_s^{(2)}$ upon varying the $E_s^{(2)} : E_p^{(1)}$ ratio; highest photoacoustic intensity at $E_s^{(2)} : E_p^{(1)} =$

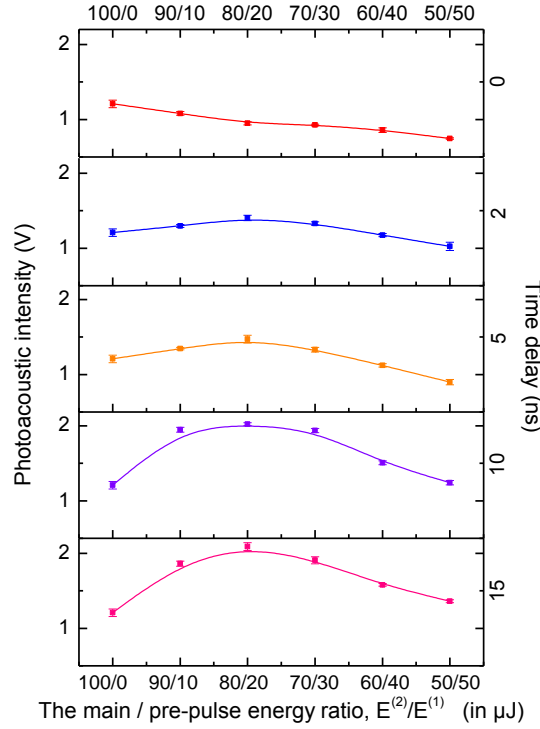


Fig. 3. Pulse energy ratios with the same total fluence as a function of photoacoustic intensity at different time delays. The delay time between the pre-pulse and main pulse was varied from 0, 2, 5, 10 and 15 ns. A total fluence of 100 μJ was used in the experiments. Lines are drawn as eye guides.

100:0 μJ and lowest at $E_s^{(2)}: E_p^{(1)} = 50:50 \mu\text{J}$. Photoacoustic intensity is dependent on the main pulse energy. When the time delay between the main pulse $E_s^{(2)}$ and pre-pulse $E_p^{(1)}$ increase from $\Delta t = 2$ to 15 ns, a noticeable peak at $E_s^{(2)}: E_p^{(1)} = 80:20 \mu\text{J}$ starts to grow from $\Delta t = 2$ ns and reaches its maximum intensity at $\Delta t = 15$ ns. The $E_s^{(2)}: E_p^{(1)} = 80:20 \mu\text{J}$ was found to be the optimal ratio with the highest enhancement in photoacoustic intensity. Accordingly, with $E_s^{(2)}: E_p^{(1)} = 80:20 \mu\text{J}$ at $\Delta t = 15$ ns, the maximum enhancement in photoacoustic intensity was achieved which is ascribed to the bubble generation in the nanosecond time scale. The photoacoustic signal growing in two recognizable shorter ~ 2 ns and longer ~ 15 ns stages [Fig. (2)], which is consistent with light scattering data (Sec. 3.2). Light scattering is sensitive to the volume of the optically excited region, i.e., nano-bubbles and nanoparticles. The saturation of photoacoustic signal reached at the end of 15 ns was at the limit of the utilised delay line, however, further increase is not expected due to the observed scattering decay with the ~ 17 ns time constant (Sec. 3.2) and the known strong damping of nano-bubble oscillation and their short lifetime of up to few nanoseconds when nanoparticles of similar size were used [19].

3.2. Bubble generation by femtosecond double-pulse

In the early stage of excitation by fs-laser pulses which occurs in several picosecond time scale after electron-ion thermalization, pre-pulse plays an important role in the thermal excitation

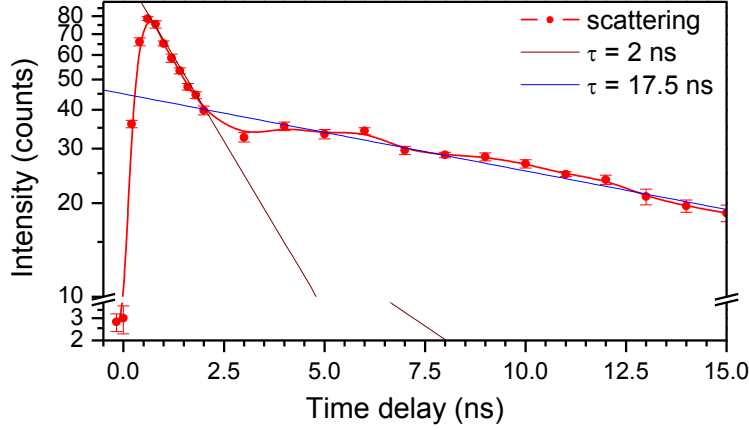


Fig. 4. Pre-pulse scattering intensity at the $\lambda = 600$ nm wavelength measured from 0 to 15 ns time delay between the pulses. A supercontinuum white light generated by fs-laser was used as strobe light to perform dark-field imaging and scattering measurements. Two single exponential decays with time constants $\tau = 2, 17.5$ ns are shown as best fits.

dynamics. The pre-pulse of the double delayed fs-laser pulses clearly affected the total laser energy coupling into gold nanoparticles and finally the ablation characteristics. To study the behavior of pre-pulse from 0 to 15 ns, the pulse energy was kept at $100 \mu\text{J}$ and the dynamics was investigated. Figure 4 shows the pre-pulse scattering intensity as a function of time delay between the pulses. At 0 to 2 ns, a rapid increase in the scattering intensity was observed due to the nanoparticle ablation and nano-bubble generation. A single-exponential decay with 17.5 ns time constant was observed after initial faster 2 ns decay.

For the focusing objective lens with numerical aperture $NA = 0.28$, the diameter of the focal spot is $2w_0 = 1.22\lambda/NA = 3.5 \mu\text{m}$. The 2 ns slope in the light side-scattering transient [Fig. (4)] can be considered as nano-bubble initiation out of the focal volume. Theoretical axial extent of the focal volume can be estimated as a double Rayleigh length $2z_R = 2n \frac{\lambda}{NA^2} = 27.1 \mu\text{m}$ and is close to the estimate made above for pressure traverse time of 17.5 ns; $n = 1.33$ is the refractive index of water. In the previous single pulse excitation photoacoustic and X-ray generation experiments, the side view images of the optically excited expanding volume had an axial extent of $\sim 30 \mu\text{m}$ at $E^{(1)} = 30 \mu\text{J}$ [33].

4. Discussion

Separation between gold nanoparticles in solution was only $\sim 1.4 \mu\text{m}$ which is smaller than $30 \mu\text{m}$ when growth of nano-bubbles is independent [47]. Size of nano-bubbles measured with X-ray scattering and shadowgraphy was around $1 \mu\text{m}$ diameter for ~ 40 -nm-diameter nanoparticles at typical range of pulse fluences 0.1 - 0.3 J/cm^2 when nanosecond laser pulses were used [17, 19]. For femtosecond laser pulses, the threshold of bubble formation is only twice lower for the optimum size for the lowest threshold of nano-bubble initiation with a wide minimum at 40 - 60 nm diameters [16, 19]. It is defined by the plasmonic scattering and absorption

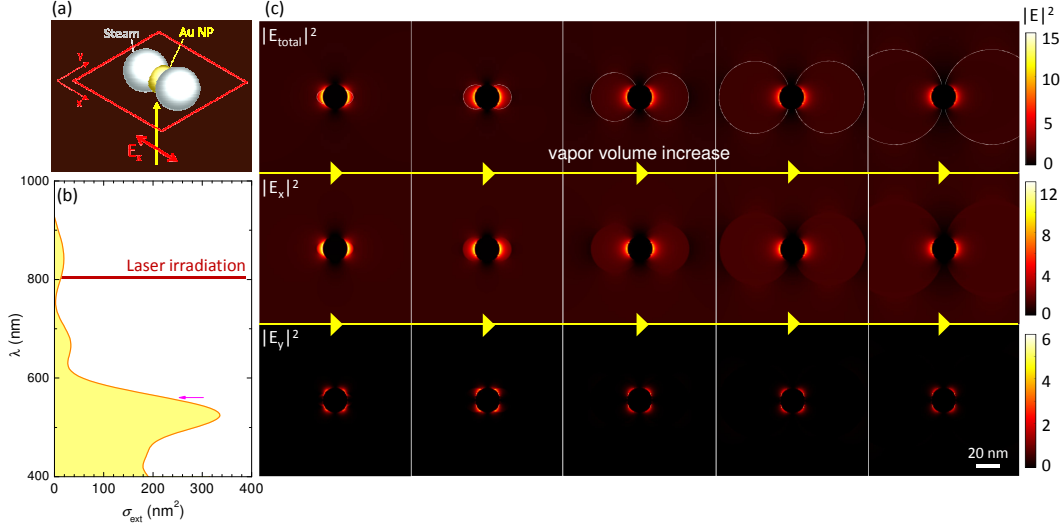


Fig. 5. (a) Schematic representation of the simulation geometry, with 800 nm wavelength light incident along z-axis and is linearly polarized along x-axis. (b) Simulated extinction cross section, σ_{ext} , spectrum of the 20 nm diameter Au nanoparticle. The arrow marks the wavelength where two-photon absorption has maximum $\sim 0.7\lambda_{ex} = 560$ nm [50]. (c) Evolution of the absolute ($|E_{total}|^2$) as well as the $|E_x|^2$ and $|E_y|^2$ component electric field intensity profiles in the x-y plane around the nanoparticle as the bubbles expand. The intensity of the $|E_z|^2$ components is three orders of magnitude lower, hence their plots are omitted.

contributions to extinction and Kapitza resistance at the nanoparticle-water interface which is responsible for a significant overheating of the nanoparticle. The observed 2 ns time constant in light scattering is consistent with the initial stages of nano-bubble growth reported in literature [18, 48, 49]. The long ~ 17 ns decay is caused by bubble growth which has typical times of 15-25 ns and is longer for the higher fluence [17]. At the used high density solution, the pressure waves from adjacent bubbles (nanoparticles) inhibits bubble growth [47], but provides a homogenised volume of high pressure as a source of photoacoustic signal.

Another feature specific to this study is very high pulse fluence ~ 1 kJ/cm² far exceeding that typical for nano-bubble formation and cell perforation at < 0.1 J/cm² [20]. At such high intensity, air breakdown at the air-water interface, white light continuum generation, and filamentation are all contributing to significant reduction of the light intensity reaching the nanoparticle. It was established that once 0.24 J/cm² fluence is exceeded, a repeated irradiation of the same nanoparticle did not produce nano-bubbles [17]. Particle reshaping and resizing was observed. We used flow of nanoparticles and the entire volume of the irradiated solution was smaller than 10% after entire experiment. Extinction spectra measured before and after photoacoustic measurements had the same spectral shape. Ablation and disintegration of nanoparticles can explain the observation. Initiation of nano-bubbles by plasma and electronic emission at the surface of nanoparticle was demonstrated for fs-laser pulses as an alternative to thermally initiated spinoidal water decomposition at strong overheating conditions typical for nanosecond pulsed irradiation [49]. Surface plasma emission from the light field enhancement locations (hot-spots) is relevant mechanism at the used high irradiance by fs-laser pulses employed in our study. Creation of hot-spots with light field enhancement by several times was modeled

numerically.

Figure 5 shows finite-difference time-domain (FDTD) simulation results of light intensity distribution for a 20 nm diameter Au nanoparticle suspended in water, assuming that plasmonic hot-spots induce nano-bubble formation around localized high intensity regions, hence, the dipolar pattern of the vapor volume. Initial stages of nano-bubble generation are taken and the light field enhancement is shown for the major components of the E-field. The time estimate for pressure wave travel 20 nm in water takes ~ 13.5 ps at velocity of sound and can be few times faster at shock wave conditions typical for such experiments [19, 48]; this can be considered as a bubble initiation time. It is evident [Fig. (5)] that, there is no new energy deposition possibilities due to opening of vapor volumes around nanoparticles via an augmented light enhancement nor due to a resonant absorption at the interfaces liquid-vapor and gold-vapor which can be important in polarized double-pulsed experiment [51]; calculations were also carried out for spherical and toroidal volumes, however, there were no significant differences. However, this modeling is not capturing presence of plasma and conditions of white light continuum. In actual experiments additional energy deposition channels also exist via two photon absorption TPA [Fig. 5(b)] and opens an efficient energy deposition. The extinction cross section has a major component at TPA wavelength [Fig. 5(b)]. Due to absorption dominance in extinction $\sigma_{ext} = \sigma_{abs} + \sigma_{sc} \simeq \sigma_{abs}$ the scattering and reflection for particles with diameter smaller than ~ 40 nm are considerably weaker [32].

Future studies of high-density solutions of nanoparticles within a small focal volume of excitation should provide optimized solutions for photoacoustic sources.

5. Conclusion

Double-pulsed fs laser irradiation to gold nanosphere colloidal suspension demonstrated a significant increase in photoacoustic intensity from 0 to 15 ns time scale. An efficient enhancement factor of ~ 2 was achieved when the pre-pulse energy is 20-30% of the total energy. The initial stage of thermal expansion and bubble generation in the nanosecond time scale were maximized under double-pulsed femtosecond excitation, leading to a significant photoacoustic enhancement. The pre-pulse of the time-delayed fs-laser pulses affected the total laser energy coupling to gold nanoparticles and thereby enhancing the ablation and photoacoustic characteristics.

Acknowledgment

TY acknowledges the partial support of Murata Foundation.

Funding

SJ is grateful for partial support via the Australian Research Council DP170100131 Discovery project and by the nanotechnology ambassador fellowship program at the Melbourne Centre for Nanofabrication (MCN) in the Victorian Node of the Australian National Fabrication Facility (ANFF).